NOTES

Magnetic Resonance in Medicine 55:1164–1169 (2006)

Unaliasing Lipid Contamination for MR Spectroscopic Imaging of Gliomas at 3T Using Sensitivity Encoding (SENSE)

Esin Ozturk-Isik,[1,2] Jason C. Crane,[2] Soonmee Cha,[2,3] Susan M. Chang,[3] Mitchel S. Berger,[3] and Sarah J. Nelson[1,2,4]

3D magnetic resonance spectroscopic imaging (MRSI) has been successfully employed to extract information about brain tumor metabolism, such as cell membrane breakdown, cellular energetics, and neuronal integrity, through its ability to differentiate signals coming from choline (Cho), creatine (Cr), and N-acetyl aspartate (NAA) molecules. The additional presence of lipids within subregions of the tumor may indicate cellular membrane breakdown due to cell death. Another potential source of lipids is subcutaneous fat, which may be excited with point-resolved spectroscopy (PRESS) volume selection and aliased into the spectral field of view (FOV) due to the chemical shift artifact and the low bandwidth of the selection pulses. The purpose of our study was to employ a postprocessing method for unaliasing lipid resonances originating from in-slice subcutaneous lipids from the 3D MRSI of gliomas at 3T, using an eight-channel phased-array coil and sensitivity encoding (SENSE). Magn Reson Med 55:1164–1169, 2006. © 2006 Wiley-Liss, Inc.

Key words: glioma; MR spectroscopic imaging; parallel imaging; SENSE; lipid

Localization and characterization of brain tumors are vital for selecting the most effective treatment from among surgical resection, radiation therapy, and chemotherapy. Pre- and postcontrast T_1-weighted imaging and T_2-weighted fluid attenuated inversion recovery (FLAIR) are the two most common types of MRI sequences used for tumor localization. Tumor is usually seen as a hypointense area in T_1-weighted images before Gd-DTPA injection. After contrast administration, Gd-DTPA leaks into the areas of the brain where the blood–brain barrier is disrupted, resulting in hyperintense regions due to the shortening of T_1. T_2-weighted FLAIR images show hyperintensity in areas of tumor, edema, and necrosis due to increased water content. Although MRI is highly sensitive for tumor detection, it may be difficult to assess the true margin of the tumor border, such as in gliomas. This is in part because gliomas exhibit an infiltrative growth pattern into adjacent normal brain tissue, and therefore often do not have grossly or macroscopically definable margins.

3D MR spectroscopic imaging (MRSI) has been proposed as a noninvasive technique that provides metabolic maps of choline-containing compounds (Cho), creatine (Cr), N-acetylaspartate (NAA), lactate (Lac), and lipid for better tumor localization and quantitative assessment of the brain metabolism (1). Previous studies suggested that the combination of MRI and MRSI is more effective in tumor staging (2), assessment of progression (3), and treatment response (4) than MRI alone. These studies indicated that Lac and lipid play an important role in distinguishing between high- and low-grade lesions and in defining necrosis (2,4). While lipid may indicate cellular membrane breakdown due to necrosis, it is also present in adipose tissue of the scalp, and if care is not taken in the data acquisition, it may be aliased into the selected volume instead of being present in the tumor.

Although imaging at high field presents many advantages, the increased chemical shift artifact may result in more severe problems with lipid resonances aliasing into the spectral FOV and compromising the quantification of Lac and NAA. Previous studies have suggested a number of methods for suppressing or reducing unwanted lipid during data acquisition, including the use of inversion recovery sequences (5), very selective suppression (VSS) pulses (6), variable-density spiral imaging (7), echo-planar spectroscopic imaging (EPSI) (8), and spectral spatial pulses (9). Postprocessing approaches have also been proposed to remove lipid using time domain fitting (10) or data extrapolation (11).

In this study we propose a relatively simple and alternative postprocessing method that uses sensitivity encoding (SENSE) (12) to reduce contamination from aliasing lipid resonances that originate from in-slice subcutaneous lipid for 3D MRSI of the brain. This was designed to be effective for data acquired at 3T using an eight-channel RF coil with point-resolved spectroscopy (PRESS) (9) localization with chemical shift-selective

[1]UCSF/UCB Joint Graduate Group in Bioengineering, University of California–San Francisco, San Francisco, California, USA.

[2]Department of Radiology, University of California–San Francisco, San Francisco, California, USA.

[3]Department of Neurosurgery, University of California–San Francisco, San Francisco, California, USA.

[4]Program in Bioengineering, University of California–San Francisco, San Francisco, California, USA.

Grant sponsor: NIH; Grant number: P50 CA9729; Grant sponsor: UC Discovery Program/GE Healthcare; Grant number: LSIT 01-10107.

Presented in part at the 13th Annual Meeting of ISMRM, Miami Beach, FL, USA, 2005.

*Correspondence to: Esin Ozturk-Isik, Surbeck Laboratory of Advanced Imaging, QB3 Building 3rd Floor, Suite 303, 1700 4th St., San Francisco, CA 94143-2532. E-mail: esin.ozturk@mrsc.ucsf.edu

Received 13 July 2005; revised 1 December 2005; accepted 11 January 2006.
DOI 10.1002/mrm.20860
Published online 4 April 2006 in Wiley InterScience (www.interscience.wiley.com).

saturation (CHESS) pulses (9) for water suppression, and VSS pulses for improved outer volume signal suppression. The performance of the technique was assessed using empirical data from a phantom and results from patients with gliomas.

MATERIALS AND METHODS

Data Acquisition

Spectroscopic imaging experiments were carried out on a uniform MRS phantom and 12 glioma patients (six grade II, one grade III, and five grade IV; six males and six females, mean age = 47 years) on a 3 T GE Signa EXCITE scanner (GE Healthcare, Milwaukee, WI, USA) equipped with an eight-channel RF coil (MRI Devices Inc., Gainesville, FL, USA). Informed consent was obtained from the patients prior to scanning. The MRS phantom contained major metabolites observed in the brain (i.e., Cho, Cr, NAA, and Lac), and there was no lipid present inside the phantom. A balloon filled with cooking oil was attached to one side of the phantom to create an artificial lipid environment. The imaging protocol included the acquisition of T_1-weighted 3D SPGR (TR = 26 ms, TE = 3 ms, slice thickness = 3 mm, matrix = 256 × 256, FOV = 240 × 240 mm, flip angle = 40°), T_2-weighted FLAIR (TR = 10002 ms, TE = 127 ms, TI = 2200 ms, slice thickness = 3 mm, matrix = 256 × 256, FOV = 240 × 240 mm, flip angle = 90°), and proton density (PD)-weighted fast gradient-echo coil sensitivity images (TR = 150 ms, TE = 2.1 ms, slice thickness = 3 mm, matrix = 64 × 64, FOV = 300 × 300 mm, flip angle = 20°). ^{1}H 3D MRSI data were acquired using PRESS volume localization with CHESS water suppression. The PRESS pulses had a bandwidth of 2400 Hz for the 90° pulse and 933 Hz for the 180° pulses. The 90° pulse was played along the anterior–posterior (AP) direction, and the two 180° pulses were played along the right–left (RL) and superior–inferior (SI) directions. The center frequency was set to be 220 Hz upfield from the water frequency so that the selected volumes for the metabolites of interest would be close to the desired region of interest (ROI). The actual PRESS-excited region was 1.2 times larger than the prescribed region (i.e., the "overpress" factor (9) was 1.2). The signal outside the prescribed region was later suppressed using the high-bandwidth VSS pulses. The combination of the overpress excitation and VSS pulses created a more homogenous excitation of the different metabolites over the FOV, and reduced the effects of the chemical shift artifact on relative peak intensities. The spectral array dimensions were 12 × 12 × 8 (N = 4) or 16 × 16 × 8 (N = 8) with 1-cc nominal spatial resolution. The rectilinear k-space sampling was restricted to a central elliptical region to reduce the scan time to 9 min for the 12 × 12 × 8 array, and 17 min for the 16 × 16 × 8 array, with TR = 1.1 s. The phantom and patient spectra were acquired with TE = 144 ms, and four patients imaged with the 12 × 12 × 8 spectral array also underwent another spectral acquisition with TE = 40 ms for a long- and short-TE spectral comparison.

Data Processing

The chemical shift artifact effects on the excitation profiles of different metabolites were estimated as follows (9):

$$\Delta x = \frac{(w - w_o)}{BW_{pulse}} \times (X_{box}), \quad [1]$$

where Δx is the spatial shift of the excitation profile for a metabolite with resonance frequency w, from the center frequency, w_o, excitation profile; BW_{pulse} is the bandwidth of the PRESS RF excitation pulse in the given direction; and X_{box} is the width of the total excited spectral region.

SENSE was successfully applied by Dydak et al. (13) to reconstruct reduced k-space data acquired with multichannel radiofrequency (RF) coils and to analyze spectroscopy data. In this study we implemented a similar approach as a postprocessing step for our 3D MRSI data by assuming that the intended FOV for our acquisition was twice as large as the one that was actually used. Following the notation of Pruessmann et al. (12), if the k-space data are reduced by a factor of R, each pixel, a, in the resulting aliased image of a channel is a superposition of pixels v_r (where $r = 1. . .R$) that are weighted by their respective coil sensitivities, s_r, as:

$$a = \sum_{r=1}^{R} s_r v_r. \quad [2]$$

It is possible to extend Eq. [2] to include all of the coil elements and represent it in a matrix multiplication form. The pseudoinverse of the sensitivity matrix, S, can be calculated and the original pixel intensities can be recovered as:

$$v = (S^H \psi^{-1} S)^{-1} S^H \psi^{-1} A, \quad [3]$$

where S^H is the complex conjugate transpose matrix of S, and ψ is the receiver noise matrix, which is a $n_c \times n_c$ matrix with noise variances of single coils at the diagonal, and the noise cross-correlation of the coils in the off-diagonal entries (12). Noise from the last 20 points of the spectra in the central 7 × 7 × 3 voxels in the spectral array were used to calculate the noise receiver matrix. The final noise receiver matrix was calculated by averaging the noise receiver matrices of the selected central 147 voxels.

For R = 1, the SENSE formulation can be considered as a method for combining the multichannel data using the coil sensitivities. For $R > 1$, it provides a means of unfolding the aliased data. We analyzed the effect of this algorithm on noise amplification using the geometry factor that was calculated for each unfolded pixel, i, defined as follows:

$$g_i = \sqrt{(S^H \psi^{-1} S)_{i,i}^{-1} (S^H \psi^{-1} S)_{i,i}}. \quad [4]$$

PD-weighted coil sensitivity images for each of the eight coil elements were acquired with a 30-cm FOV. Although the coil sensitivity maps were acquired with the PD weighting, there were still some anatomy-related nonuniformities, such as darker ventricle and skull regions. For unfolding the lipid we anticipated that accurate coil sensitivity estimates were necessary in the scalp and skull regions, which are the main lipid-containing regions. A software program was implemented using Matlab 6.5 (The

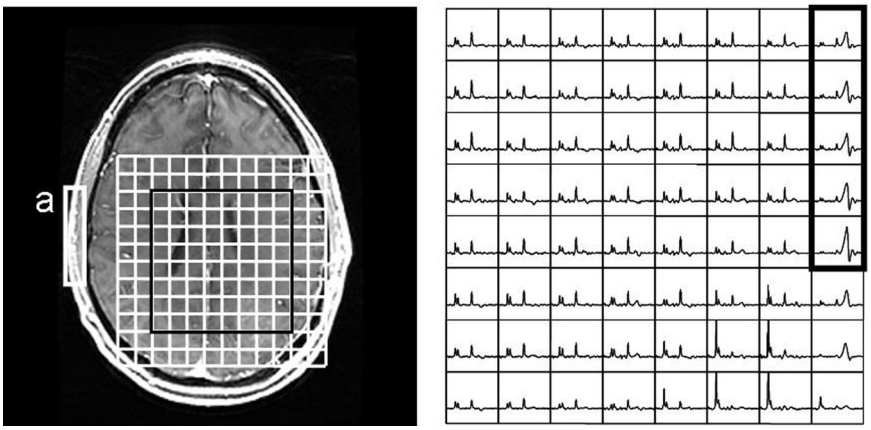

FIG. 1. Example of the lipid aliasing problem in MR spectra. Left: T_1-weighted SPGR image with the spectral FOV (white grid), and the PRESS-selected region (black box within the grid). Right: MR spectra from the PRESS-selected region. Spectral voxels marked with the black box have aliasing lipid resonances coming from the scalp region an FOV away within the white box marked with a on the image.

Mathworks Inc., Natick, MA, USA) to reduce the anatomy-related inhomogeneities of the coil sensitivity maps. The edges of the brain were found from the combined images using the Canny method to create a mask of the anatomy. Sensitivity images of the individual coil elements were masked and then divided by the combined (sum of squares) images. The resulting images were filtered with median- and low-pass homomorphic filters consecutively to smooth the image discontinuities. Coil sensitivities were resampled to twice the spectral resolution for the in-plane directions. The images were dilated by a 3×3 kernel to preserve the edges of the image before resampling.

Spectra from the eight coil elements were processed in parallel on a Linux cluster using software developed in our laboratory (9). Multichannel reconstructed spectra were combined using the coil sensitivity weighted sum (referred to as the aliased result), and the lipid unaliasing routine (unaliased). Two sets of spectra were generated for each combined data: one by phasing on the Cho peak, and the other by phasing on the lipid peak to get accurate estimates of the amount of lipid in aliased voxels without affecting the other metabolite levels. Spectral peak heights were determined from these individually phased spectral sets. Lipid-contaminated voxels were determined by selecting the voxels with a lipid peak height higher than the mean Cho height for the patients' data, and higher than one-fourth of the mean Cho height for the phantom data within the selected PRESS box. Lipid heights were normalized with the mean Cho height within the PRESS box for both the aliased and unaliased datasets. A Wilcoxon sign-rank test was used to assess whether the levels of normalized lipid within the contaminated voxels were significantly reduced by utilizing the unaliasing routine. P-values < 0.05 were considered significant.

RESULTS

Figure 1 shows an example of the spectral lipid aliasing problem. The lipid peaks seen on the right edge of the PRESS box were thought to originate from the scalp on the left side of the head, as a result of the chemical shift artifact. This assumption was supported by the calculation of the lipid PRESS box location. Using an 80-mm spectral box selection along the RL direction with a 1.2 overpress factor, 933 Hz bandwidth of the RF pulse, 220 Hz shift of lipid from the center frequency, and the directionality information of the chemical shift artifact, the lipid excitation profile could then be estimated to be shifted from the center frequency excitation profile by 22.6 mm toward the left-hand side. This would result in the excitation of the relatively large lipid signals at the indicated subcutaneous fat region, and their aliasing to the other end of the PRESS box due to the small spectral FOV. Although the VSS pulses are used for effective suppression of the relatively low metabolite signals outside the PRESS box, they may not be able to fully suppress the high lipid signal in the scalp region, and can result in aliasing of the spectral signals as shown in this example.

Elements of the eight-channel RF coil were overlapped to minimize the mutual inductance among neighboring elements, and low-impedance preamplifiers were utilized

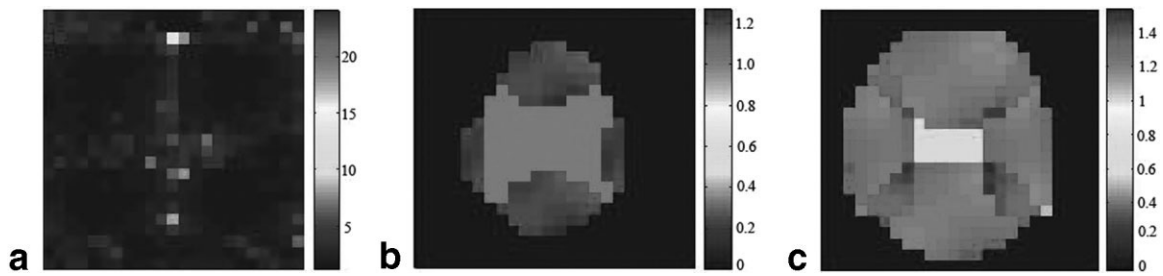

FIG. 2. Geometry factor maps before (**a**) and after (**b**) the object region was masked, and after the full coil sensitivity map correction was performed (**c**).

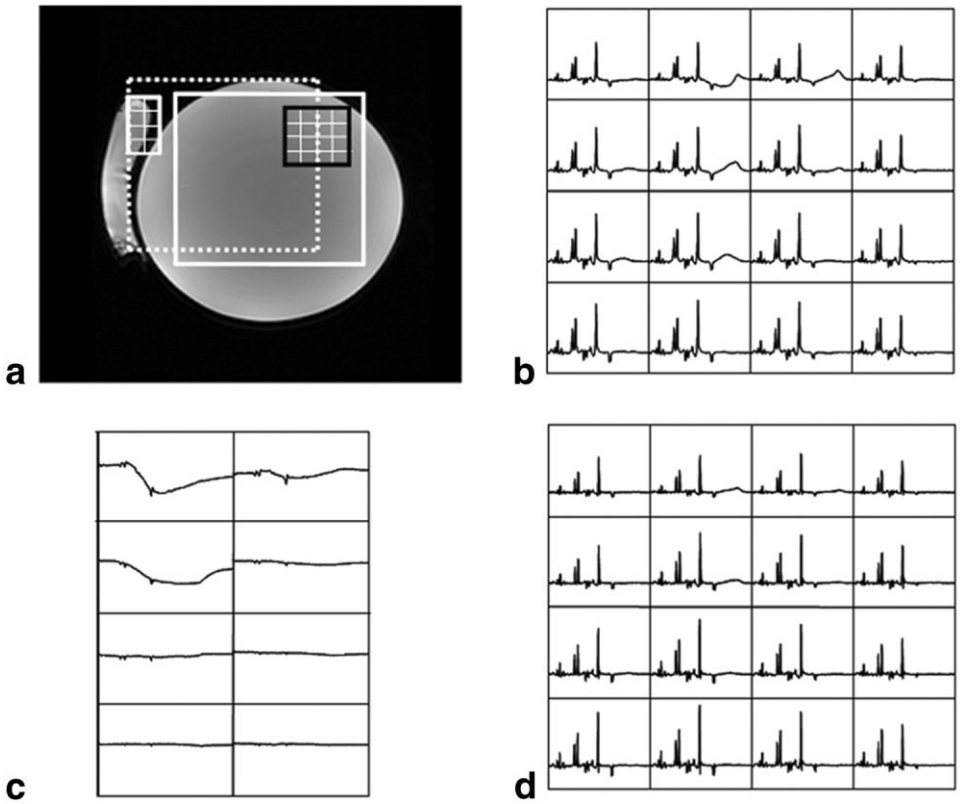

FIG. 3. (**a**) Phantom with the lipid-filled balloon attached to the left side. The PRESS-excited region for the center frequency (white box) and lipid frequency (dotted box), lipid-contaminated region in the PRESS selection (black box), and unfolded lipid regions (small white grid on the balloon) are marked on the image. MR spectra from the black box before (**b**) and after (**d**) lipid unaliasing, and the lipid spectra unfolded into the white grid that is an FOV away from the black box region (**c**) are also shown.

to minimize the interaction with the next-nearest and distant neighbors (14). Inductive decoupling solenoids were also present to further reduce coupling between an element and the next-nearest neighbor. It was observed that the noise receiver matrix had high intensities ranging from 0.54–1 for the phantom and 0.72–1 for sample glioma patient data in the diagonal entries, and much smaller values ranging from 0.08–0.34 for the phantom and 0.004–0.27 for the glioma patient data in the off-diagonal entries.

Figure 2 shows the geometry factor maps that were calculated from a slice of a patient data set before and after the coil sensitivity maps were masked on the left and center, respectively, and after the coil map correction algorithm was applied on the right. Our findings confirm that the geometry factors were very high before the coil sensitivity images (15) were masked with a local maximum of 24.16, because the true degree of aliasing was not correctly estimated. Geometry factors in the central 25 voxels of the brain ranged from 1.67–5.70. After masking, it was observed that the geometry factors were smaller, with a range of 1–1.27 in the head region. The coil sensitivity correction algorithm was necessary to reduce anatomy-related nonuniformities in the coil sensitivity images and preserve the edges of the head region so that lipid unaliasing could be successfully applied. It was observed that the coil sensitivity correction increased the geometry factors, especially in the coil overlapping sections, but the maximum value still stayed under 1.55, which was regarded as being relatively favorable.

Figure 3a shows an axial slice through the MRS phantom with the lipid balloon attached to the left-hand side. Fourteen lipid-contaminated voxels were identified within the PRESS volume. The PRESS-excited region for the center frequency is marked with the big white box, and the corresponding lipid-excited region due to the chemical shift artifact is marked with the box with dotted lines. Figure 3b and d show spectra from the black box before and after the lipid unaliasing, respectively. Figure 3c shows the lipid spectra within the white grid located on the lipid-filled balloon region calculated by the unaliasing algorithm. It was found that the unaliasing routines significantly ($P < 0.001$) reduced the normalized lipid heights within the original spectral FOV. The normalized lipid heights were reduced by a median of 91% ± 34% (median ± standard deviation (SD)). The maximum and minimum reductions of the normalized lipid heights were 100% and 13%, respectively.

The average number of lipid-contaminated voxels across patients for the $12 \times 12 \times 8$ array size spectra was 88 ± 37 for the short TE, and 76 ± 37 for the long TE. The $16 \times 16 \times 8$ array size resulted in much less lipid contamination overall, with an average of 14 ± 12 lipid-contaminated voxels. The lipid unaliasing algorithm reduced the total normalized lipid peak height by a median of 41% ± 7% (min = 29%, max = 47%) for the $12 \times 12 \times 8$ short-TE, 45% ± 10% (min = 41%, max = 63%) for the $12 \times 12 \times 8$ long-TE, and 52% ± 21% (min = 19%, max = 74%) for the $16 \times 16 \times 8$ long-TE spectra. Lipid unaliasing was significant ($P < 0.05$) for all four short-TE spectra, and for 10 of the 12 long-TE spectra. The array size was $16 \times 16 \times 8$ for the two cases in which the lipid unaliasing was not significant, and the spectra had only one and two lipid-contaminated voxels, respectively.

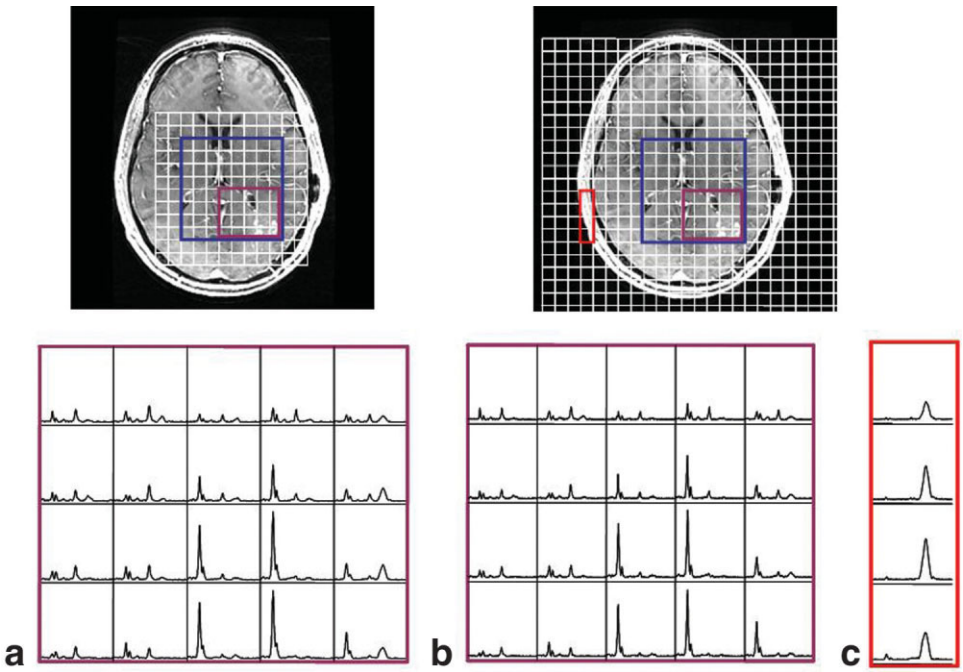

FIG. 4. Example of data from a glioma patient. Top left: T_1-weighted SPGR image of a slice with the spectral FOV (white grid), a PRESS-selected region (blue box), and a region with lipid-contaminated voxels (purple box). Top right: Same image slice with the extended spectral FOV through the unaliasing algorithm (white grid) and the correctly located lipid region (red box). Also shown are spectra of the purple box before (**a**) and after (**b**) lipid unaliasing, and the lipid spectra unaliased into the red box that is an FOV away (**c**).

Figure 4 shows an example of the results for a glioma patient. The original spectral FOV is shown on the top left, and the extended FOV is shown on the top right image with the white grids. The blue box represents the PRESS-excited volume, and the purple box marks the lipid-contaminated areas. Figure 4a and b show spectra before and after the unaliasing procedure, respectively. The small red box in the scalp region on the top-right image marks the lipid unfolded areas, and Fig. 4c shows the spectra unfolded into this region. The unaliasing algorithm significantly reduced the normalized lipid heights in individual voxels by a median of 40% ± 17% for this patient. The maximum and minimum reductions of normalized lipid heights at a given voxel were 76% and 10%, respectively.

DISCUSSION

This study presents a postprocessing method for reducing lipid aliasing for 3D MRSI acquired with multichannel RF coils with small FOV without requiring the implementation of special pulse sequences. The algorithm was effective in removing aliased lipid peaks, and took only 2–3 min on a Sun Blade 1000 Workstation for a 12 × 12 × 8 MRSI dataset. This technique detected aliasing problems and resolved only the aliasing lipids without affecting other metabolites, such as Lac, that resonate at similar frequencies. Results from phantoms showed that an underlying lipid peak tail can affect the Lac peak height and area estimates, and that removal of the nonresident lipid peaks would result in more reliable Lac quantification using the frequency domain-based methods.

In-slice lipid contamination was more severe in the RL and SI directions compared to the AP direction, due to the smaller bandwidth of the PRESS spectral volume excitation pulse in those directions. In addition to this effect, along the RL direction the lipid resonances on the left side of the PRESS volume were excited more due to the directionality of the chemical shift artifact. This resulted in more contamination on the right side of the spectral array. The higher bandwidth pulse in the AP direction meant that the lipid regions in the orbits and the narrowing scalp and skull were minimally excited. An alternative approach for reducing the chemical shift artifact would be to use higher bandwidth volume selection pulses. Spectral spatial pulses that have high bandwidths of 5000 Hz would have reduced the chemical shift artifact by more than four times in the 180°-pulse direction, and two times in the 90°-pulse direction. A limitation of such pulses is that they are relatively long and cannot be used to obtain short-TE data.

The lipid aliasing was more prominent for the smaller 12 × 12 × 8 matrix size because there were lipid-containing areas just outside the spectral FOV that were close enough to be affected by the chemical shift artifact. Lipid aliasing was less prominent in the 16 × 16 × 8 arrays, because the larger FOV covered the whole head in the RL direction in most cases. Although increasing the matrix size does reduce the aliasing, the 12 × 12 × 8 array is preferred because it provides a clinically significant reduction in scan time and could be valuable for enabling the acquisition of multiple spectral data sets from a patient on the same day. Another factor that affected the severity of the aliasing artifact was the location and size of the PRESS-selected region, with more central and smaller boxes having a reduced effect. Although the short-TE spectra had higher lipid contamination in more voxels compared to longer-TE spectra, the lipid unaliasing algorithm was similarly efficient in reducing the aliasing lipids for both cases.

The lipid unaliasing algorithm may be further improved by reducing matrix inversion errors caused by the possible ill conditioning of the overdetermined system using regularization techniques (16). Regularization methods, such as Tikhonov's regularization or the conjugate gradient

method, have been proposed to generate approximate objects that are compatible with the given data by using a priori information and energy and bias restrictions explicitly (17). Although regularization algorithms might condition the matrix inversion, this may not solve the problem completely if there are data- or system definition-related problems. One problem area that could cause the inversion errors would be the use of the original coil sensitivity maps, which are known to have anatomy-related contrast that diverges from the actual sensitivity values. By smoothing the coil sensitivity maps as suggested, we believed these errors can be minimized.

Another reason for the presence of residual lipid peaks in the empirical data was that the lipid unfolding could only be applied in two dimensions. The PRESS pulses used in this study had a 180° pulse with 933 Hz bandwidth in the SI direction, and hence the scalp and skull regions in the superior or inferior directions could also cause lipid aliasing. However, the phased-array head coil used in this study was composed of eight elements that were aligned with the *z*-direction in the magnet bore, and hence there was differential coil sensitivity only along the axial directions. An alternative approach for reducing lipid contamination in the SI direction would be to increase the FOV in that direction using alternative spatial encoding, such as EPSI. This approach would reduce the acquisition time while still allowing the use of a larger data matrix. The combination of an enlarged FOV and the lipid unaliasing algorithm would further enhance the overall performance on empirical data.

The SENSE algorithm was previously applied to enable scan time reduction for MRS (13) and resolve image aliasing problems (18,19). In the present study we integrated those two distinct applications of the SENSE algorithm to resolve the problem of lipid aliasing in the RL and AP directions. A possible extension of this approach would be to apply the lipid unaliasing to a reduced *k*-space data set. The SENSE algorithm would be applied twice to solve for both aliasing types stemming from the data reduction, and the chemical shift artifact. A recently published study reported that the SENSE algorithm may not perform optimally when aliasing occurs due to a small FOV in the data prior to reduction (20), and further studies will examine the implications of this strategy for spectral imaging of gliomas. Unaliasing lipid resonances is likely to enable more reliable quantification of MRS data, more accurate assessment of the metabolic state of brain tumors, and improved characterization of changes due to therapy and progression for patients with gliomas.

ACKNOWLEDGMENTS

The authors thank Daniel B. Vigneron, Ph.D., Susan M. Noworolski, Ph.D., Suchandrima Banerjee, Janine M. Lupo, Michael C. Lee, Ph.D., Lucas Carjaval, Julio Carballido, Duan Xu, Ph.D., Albert Chen, Joseph Osorio, Rebeca Choy, Bert Jimenez, and Niles Bruce for useful discussions and help during various stages of the data acquisition and processing.

REFERENCES

1. Nelson SJ. Multivoxel magnetic resonance spectroscopy of brain tumors. Mol Cancer Ther 2003;2:497–507.
2. Li X, Lu Y, Pirzkall A, McKnight T, Nelson SJ. Analysis of the spatial characteristics of metabolic abnormalities in newly diagnosed glioma patients. J Magn Reson Imaging 2002;16:229–237.
3. Graves EE, Nelson SJ, Vigneron DB, Verhey L, McDermott M, Larson D, Chang S, Prados MD, Dillon WP. Serial proton MR spectroscopic imaging of recurrent malignant gliomas after gamma knife radiosurgery. AJNR Am J Neuroradiol 2001;22:613–624.
4. Nelson SJ, Huhn S, Vigneron DB, Day MR, Wald LL, Prados M, Chang S, Gutin PH, Sneed PK, Verhey L, Hawkins RA, Dillon WP. Volume MRI and MRSI techniques for the quantitation of treatment response in brain tumors: presentation of a detailed case study. J Magn Reson Imaging 1997;7:1146–1152.
5. Spielman DM, Pauly JM, Macovski A, Glover GH, Enzmann DR. Lipid-suppressed single- and multisection proton spectroscopic imaging of the human brain. J Magn Reson Imaging 1992;2:253–262.
6. Tran TK, Vigneron DB, Sailasuta N, Tropp J, Le Roux P, Kurhanewicz J, Nelson S, Hurd R. Very selective suppression pulses for clinical MRSI studies of brain and prostate cancer. Magn Reson Med 2000;43:23–33.
7. Adalsteinsson E, Star-Lack J, Meyer CH, Spielman DM. Reduced spatial side lobes in chemical-shift imaging. Magn Reson Med 1999;42:314–323.
8. Ebel A, Maudsley AA. Comparison of methods for reduction of lipid contamination for in vivo proton MR spectroscopic imaging of the brain. Magn Reson Med 2001;46:706–712.
9. Nelson SJ. Analysis of volume MRI and MR spectroscopic imaging data for the evaluation of patients with brain tumors. Magn Reson Med 2001;46:228–239.
10. de Beer R, Michels F, van Ormondt D, van Tongeren BP, Luyten PR, van Vroonhoven H. Reduced lipid contamination in in vivo 1H MRSI using time-domain fitting and neural network classification. Magn Reson Imaging 1993;11:1019–1026.
11. Haupt CI, Schuff N, Weiner MW, Maudsley AA. Removal of lipid artifacts in 1H spectroscopic imaging by data extrapolation. Magn Reson Med 1996;35:678–687.
12. Pruessmann KP, Weiger M, Scheidegger MB, Boesiger P. SENSE: sensitivity encoding for fast MRI. Magn Reson Med 1999;42:952–962.
13. Dydak U, Weiger M, Pruessmann KP, Meier D, Boesiger P. Sensitivity-encoded spectroscopic imaging. Magn Reson Med 2001;46:713–722.
14. Roemer PB, Edelstein WA, Hayes CE, Souza SP, Mueller OM. The NMR phased array. Magn Reson Med 1990;16:192–225.
15. Weiger M, Pruessmann KP, Leussler C, Roschmann P, Boesiger P. Specific coil design for SENSE: a six-element cardiac array. Magn Reson Med 2001;45:495–504.
16. Lin FH, Kwong KK, Belliveau JW, Wald LL. Parallel imaging reconstruction using automatic regularization. Magn Reson Med 2004;51:559–567.
17. Bertero M, Boccacci P. Introduction to inverse problems in imaging. Bristol/Philadelphia: IOP Publishing Ltd; 1998. 351 p.
18. Kellman P, McVeigh ER. Ghost artifact cancellation using phased array processing. Magn Reson Med 2001;46:335–343.
19. Winkelmann R, Bornert P, Nehrke K, Dossel O. Efficient foldover suppression using SENSE. MAGMA 2004.
20. Griswold MA, Kannengiesser S, Heidemann RM, Wang J, Jakob PM. Field-of-view limitations in parallel imaging. Magn Reson Med 2004;52:1118–1126.